The influence of summertime convection over Southeast Asia on water vapor in the tropical stratosphere

J. S. Wright,[1] R. Fu,[2] S. Fueglistaler,[3] Y. S. Liu,[4] and Y. Zhang[5]

[1]   The relative contributions of Southeast Asian convective source regions during boreal summer to water vapor in the tropical stratosphere are examined using Lagrangian trajectories. Convective sources are identified using global observations of infrared brightness temperature at high space and time resolution, and water vapor transport is simulated using advection-condensation. Trajectory simulations are driven by three different reanalysis data sets, GMAO MERRA, ERA-Interim, and NCEP/NCAR, to establish points of consistency and evaluate the sensitivity of the results to differences in the underlying meteorological fields. All ensembles indicate that Southeast Asia is a prominent boreal summer source of tropospheric air to the tropical stratosphere. Three convective source domains are identified within Southeast Asia: the Bay of Bengal and South Asian subcontinent (MON), the South China and Philippine Seas (SCS), and the Tibetan Plateau and South Slope of the Himalayas (TIB). Water vapor transport into the stratosphere from these three domains exhibits systematic differences that are related to differences in the bulk characteristics of transport. We find air emanating from SCS to be driest, from MON slightly moister, and from TIB moistest. Analysis of pathways shows that air detrained from convection over TIB is most likely to bypass the region of minimum absolute saturation mixing ratio over the equatorial western Pacific; however, the impact of this bypass mechanism on mean water vapor in the tropical stratosphere at 68 hPa is small (<0.1 ppmv). This result contrasts with previously published hypotheses, and it highlights the challenge of properly quantifying fluxes of atmospheric humidity.

Citation: Wright, J. S., R. Fu, S. Fueglistaler, Y. S. Liu, and Y. Zhang (2011), The influence of summertime convection over Southeast Asia on water vapor in the tropical stratosphere, *J. Geophys. Res.*, *116*, D12302, doi:10.1029/2010JD015416.

1.   Introduction

[2]   Water vapor is of central importance to both chemical and radiative processes in the stratosphere. Water vapor constitutes the primary source of hydroxyl (OH) radicals in the stratosphere, and thus plays a significant role in regulating both the loss rate of stratospheric ozone and the oxidation of stratospheric methane. Furthermore, fluctuations in the distribution or amount of stratospheric water vapor have important implications for both stratospheric and surface temperature. Simulations using a variety of models show that increases in stratospheric water vapor act to enhance the loss rate of ozone, cool the lower stratosphere, and warm the Earth's surface [e.g., *Dvortsov and Solomon*, 2001; *Shindell*, 2001; *Forster and Shine*, 2002; *Stenke and Grewe*, 2005; *Solomon et al.*, 2010].

[3]   Stratospheric water vapor in the tropics exhibits a strong seasonal cycle that propagates upward with time (the 'tropical tape recorder') [*Mote et al.*, 1996]. This signal may be explained in large part by the annual cycle of zonal mean temperatures (and consequently water vapor saturation mixing ratios) at the tropical tropopause; however, the zonally asymmetric patterns of temperature, circulation, and convection also undergo large variations with seasons. These zonally asymmetric variations may also contribute substantially to the annual cycle of water vapor mixing ratios in air entering the stratosphere. Source analyses of stratospheric water vapor using global models suggest that convection in the Southeast Asian monsoon region is a primary contributor to the moist phase of the tropical tape recorder [e.g., *Bannister et al.*, 2004; *Lelieveld et al.*, 2007]. Using a Lagrangian trajectory analysis to characterize water vapor entering the stratosphere, *Fueglistaler et al.* [2005] showed that the Southeast Asian region plays two distinct roles in setting the moist phase of the tape recorder. First, Southeast Asia is the preeminent tropospheric source of air entering the tropical stratosphere during boreal summer. Second, the

[1]Department of Applied Mathematics and Theoretical Physics, University of Cambridge, Cambridge, UK.
[2]Department of Geological Sciences, University of Texas at Austin, Austin, Texas, USA.
[3]Department of Geosciences, Princeton University, Princeton, New Jersey, USA.
[4]School of Mathematics and Statistics, University of St. Andrews, North Haugh, UK.
[5]Goddard Earth Sciences and Technology Center, University of Maryland Baltimore County, Baltimore, Maryland, USA.

temperature imprint carried by water vapor entering the stratosphere is disproportionately set by conditions in the tropopause layer above Southeast Asia.

[4] The tropical tropopause is generally not considered as a material surface, but rather as a transitional layer between the troposphere and the stratosphere (the tropical tropopause layer or TTL) [*Fueglistaler et al.*, 2009a]. The lower boundary of this layer is often defined as the level of zero radiative heating (LZRH), which represents the threshold between air that is radiatively subsiding (below the LZRH) and air that is radiatively ascending (above). Observations of water vapor and its deuterated isotopologue (HDO) in the tropical lower stratosphere suggest a dominant contribution of deep convective detrainment above the LZRH, and sometimes above the cold point tropopause, followed by slow ascent [*Moyer et al.*, 1996; *Steinwagner et al.*, 2010]. Several distinct deep convective regimes are active within Southeast Asia during boreal summer. These include monsoon convection over the South Asian subcontinent and Bay of Bengal [e.g., *Petersen and Rutledge*, 2001; *James et al.*, 2008; *Devasthale and Fueglistaler*, 2010], coastal and maritime convection in the vicinity of the South China and Philippine Seas [e.g., *Petersen and Rutledge*, 2001; *Hirose and Nakamura*, 2005; *James et al.*, 2008], and continental convection over the Tibetan Plateau and South Slope of the Himalayas [e.g., *Uyeda et al.*, 2001; *Fujinami et al.*, 2005; *Fu et al.*, 2006; *Yasunari and Miwa*, 2006]. Considerable recent debate has centered around the relative contributions of convection in these subregional domains to tropical stratospheric water vapor.

[5] *Fu et al.* [2006] showed that deep convection over the Tibetan Plateau and south slope of the Himalayas is a substantial source of water vapor to the local lower stratosphere. They further suggested that transport from convection over the Tibetan Plateau and south slope of the Himalayas could represent a short-circuit of the tropical tropopause cold trap, thereby supplying relatively moist air to the global stratosphere. Boreal summer over the Tibetan Plateau is characterized by a large southwesterly influx of moist air from the South Asian subcontinent and Bay of Bengal, accompanied by strong diurnal heating [*Yasunari and Miwa*, 2006]. These conditions generate a convectively unstable atmosphere and promote the accumulation of large amounts of convective available potential energy (CAPE), with maximum daily values between 4000 and 6000 J kg^{-1} [*Liu et al.*, 2002]. Deep, intense convection occurs frequently over the Tibetan Plateau and south slope of the Himalayas during late afternoon and early evening (12:00–15:00 UTC) [*Uyeda et al.*, 2001; *Fujinami et al.*, 2005; *Hirose and Nakamura*, 2005; *Yasunari and Miwa*, 2006]. This afternoon convection can penetrate to the tropopause layer, which is both lower and warmer (order ~5 K) over the Tibetan Plateau than in the tropics [*Fu et al.*, 2006].

[6] Results of simulations using a coupled lower middle atmosphere global chemistry-climate model support the hypothesis proposed by *Fu et al.* [2006], finding that deep convection over the Tibetan Plateau and south slope of the Himalayas is highly influential in generating the moist phase of the simulated stratospheric tape recorder [*Lelieveld et al.*, 2007]. The results of other studies indicate that the Bay of Bengal and South China Sea are the dominant convective sources of moist air in the lower stratosphere over Southeast

Asia, and suggest that the influence of deep convection over the Tibetan Plateau is secondary [*Park et al.*, 2007; *James et al.*, 2008; *Devasthale and Fueglistaler*, 2010]. These latter studies consider only the influence of convection on the local lower stratosphere over Southeast Asia, as did *Fu et al.* [2006]. Other studies, such as that by *Fueglistaler et al.* [2005], have considered water vapor entering the global stratosphere but have traced it back to more general tropospheric sources, rather than directly relating it to convection.

[7] In this study, we will extend these previous studies to assess the relative contributions of distinct convective regimes within Southeast Asia to the seasonal flux of water vapor between this region and the tropical lower stratosphere. In particular, a Lagrangian back trajectory approach is used to connect the tropical lower stratosphere to its convective source regions. This allows us to identify whether and how differences in convective source location modify the interaction of trajectories with the temperature and saturation specific humidity fields, and hence water vapor transport into the stratosphere. Three distinct reanalysis data sets are used to drive the trajectory model, both to emphasize points of consistency and to evaluate the sensitivity of the results to differences in the underlying meteorological fields. Convective sources are identified as the intersection of trajectories with satellite observations of cold, optically thick, high-altitude clouds, as in work by *James et al.* [2008]. Water vapor transport is evaluated according to advection-condensation, as in work by *Fueglistaler et al.* [2005] and *Liu et al.* [2010]. Satellite observations of water vapor in the lower stratosphere are used to provide context to the results.

2. Data and Method

2.1. Trajectory Model

[8] Back trajectories are integrated using a modified version of the Goddard Fast Trajectory Model (FTRAJ) [*Schoeberl and Sparling*, 1995]. Horizontal motion along each trajectory is determined using reanalysis winds, and vertical motion is estimated using analyzed diabatic heating rates. Trajectory motion is calculated using a fourth-order Runge-Kutta integration with fifty time steps per day. Reanalysis winds and heating rates are first interpolated vertically to a potential temperature grid with approximately 1 km resolution in the tropical troposphere and stratosphere using cubic convolution. This helps to ensure that temperature minima in the tropopause layer are sufficiently cold: the coldest point of the tropical mean temperature profile is generally between 190 K and 194 K and the absolute minimum temperature in the tropics ranges from 180 K to 185 K, dependent on the reanalysis and the time of year. Winds and heating rates are linearly interpolated in space and time to the trajectory location at each time step of the trajectory integration.

[9] Three distinct ensembles of trajectories are calculated. For the first ensemble, the model is driven using winds and heating rates from the Modern Era Retrospective analysis for Research and Applications (MERRA) produced by the Global Modeling and Assimilation Office (GMAO) of the National Aeronautics and Space Administration (NASA) [*Bosilovich*, 2008]. The second ensemble is calculated using European Centre for Medium-Range Weather Forecasting (ECMWF) Interim reanalysis products (ERA-Interim)

[*Simmons et al.*, 2007]. Trajectories in the third ensemble are driven using the National Center for Environmental Prediction/National Center for Atmospheric Research (NCEP/NCAR) reanalysis [*Kalnay et al.*, 1996].

[10] The GMAO MERRA reanalysis was conceived as a satellite era reanalysis (i.e., 1979 to present), with the particular aims of providing a climate context to current generation satellite observations and improving the representation of the hydrologic cycle in reanalyses. The reanalysis is produced using version 5.0.2 of the Goddard Earth Observing System (GEOS-5) data assimilation system [*Rienecker et al.*, 2008]. MERRA products are provided by the GMAO at $1.25° \times 1.25°$ horizontal resolution and 6-hourly time resolution with 42 pressure levels. Variables in the upper troposphere and lower stratosphere (UTLS) are reported on 7 pressure levels between 300 hPa and 50 hPa. The horizontal winds and temperatures used to drive FTRAJ are diagnosed using both the model and assimilation increments, and are strongly influenced by assimilated observational data. Diabatic heating rates are determined solely by the model, and are reported on the native model grid $(0.67° \times 0.5°)$ as time means over three hour increments. The heating rate data used as inputs to FTRAJ are regridded and subsampled in time to match the spatial and temporal resolution of MERRA winds and temperatures. MERRA heating rates include heating due to shortwave and longwave radiation, moist physics, gravity wave drag, turbulence, and friction. See work by *Lucchesi* [2008] for additional information regarding the MERRA reanalysis.

[11] ERA-Interim (ERAI) winds and temperatures are provided every 6 h on 60 model hybrid sigma levels at $1° \times 1°$ horizontal resolution [*Simmons et al.*, 2007]. Variables are reported in the UTLS at higher resolution than for GMAO MERRA, with 12 levels between 300 hPa and 50 hPa. As with GMAO MERRA, winds and temperatures are strongly influenced by the assimilation data, while heating rates are determined solely by the model. ERAI heating rates are reported as integrated temperature tendencies over 6 h intervals, and are converted to mean heating rates over the interval prior to input in FTRAJ. For this analysis, we use the total diabatic heating reported by ECMWF, which includes radiative heating, latent heat exchange, and diffusive and turbulent heat transport. See work by *Fueglistaler et al.* [2009b] for a detailed examination of the ERAI diabatic heat budget in the UTLS.

[12] NCEP/NCAR reanalysis products are provided on a $2.5° \times 2.5°$ grid at 6-hourly time resolution with 17 pressure levels. Vertical resolution in the UTLS is identical to that of GMAO MERRA, with variables reported on the same 7 levels between 300 hPa and 50 hPa. Horizontal winds and temperatures are classified as category A products by the NCEP/NCAR data processing system, meaning that they are strongly influenced by observed data. Diabatic heating rates are classified as category C products, meaning that they are determined solely by model fields forced by the data assimilation. The NCEP/NCAR heating rates include heating by shortwave and longwave radiation, large-scale condensation, deep and shallow convection, and vertical diffusion. See work by *Kalnay et al.* [1996] for details on the model parameterizations that affect the heating rates. Diabatic heating rates are reported on the native model grid (T62; 28 hybrid sigma levels), and are regridded to match

the resolution of the horizontal winds and temperatures before being used as inputs to FTRAJ.

2.2. Observations of Water Vapor and Temperature

[13] Observations of water vapor and temperature are provided by the Earth Observing System (EOS) Aura Microwave Limb Sounder (MLS) [*Waters et al.*, 2006]. The MLS instrument was launched on board the Aura satellite by NASA in July 2004 and has been observing atmospheric emission in the thermal microwave (millimeter and submillimeter wavelengths) from August 2004 through the present. Observations are spaced $1.5°$ apart in latitude (165 km), roughly corresponding to the along-track resolution of temperature and water vapor in the UTLS. In this analysis, we use version 2.2 of the MLS temperature and water vapor retrievals [*Livesey et al.*, 2007] at 68 hPa.

[14] The MLS temperature product is retrieved using observations of the 118 GHz O_2 line and the 234 GHz $O^{18}O$ line [*Schwartz et al.*, 2008]. We filter the data using standard quality controls, as described by *Livesey et al.* [2007] and *Schwartz et al.* [2008]. At the 68 hPa level, the horizontal resolution of the observation is 165 km by 7 km (along track by across track), with a vertical resolution of 4 km. The estimated precision of temperature retrievals at this level is 0.8 K, and the observed bias relative to correlative observations from other sources is -1 K $\pm$ 1 K [*Schwartz et al.*, 2008].

[15] MLS water vapor at 68 hPa is retrieved using observations of atmospheric emission near the 183 GHz water vapor rotational line [*Lambert et al.*, 2007]. As with temperature, the data we use is filtered according to standard quality controls, as described by *Livesey et al.* [2007] and *Lambert et al.* [2007]. Water vapor observations at 68 hPa have a horizontal resolution of 220 km by 7 km (along track by across track), with a vertical resolution of 3.2 km. The estimated accuracy of water vapor measurements at 68 hPa is 6%. The MLS water vapor product shows very good agreement with other observational platforms at this altitude, as described by *Lambert et al.* [2007].

2.3. Observations of Convection

[16] Observations of convection are provided by the Cloud Archive User Service (CLAUS) data set [*Hodges et al.*, 2000; *Robinson and Hodges*, 2005]. CLAUS is an aggregated and gridded assimilation of infrared (IR) brightness temperatures from International Satellite Cloud Climatology Project (ISCCP) B3 data. IR brightness temperatures are observed in band 2 (~11 μm) from geostationary satellites and band 4 (10.5–11.5 μm) from the Advanced Very High Resolution Radiometer (AVHRR) on board National Oceanic and Atmospheric Administration (NOAA) polar orbiting satellites. The CLAUS data used in this study is reported on a $0.33° \times 0.33°$ uniform grid at 3-hourly temporal resolution. The average total error in IR brightness temperature is estimated to be ±3 to 4 K; details of the uncertainty estimation and data processing algorithm are given by *Robinson and Hodges* [2005].

[17] CLAUS observations of IR brightness temperature have been converted to cloud top pressure using ERAI reanalysis temperatures, which are described in section 2.1. The data is first interpolated onto pressure levels corresponding to the average model level pressure, and subse-
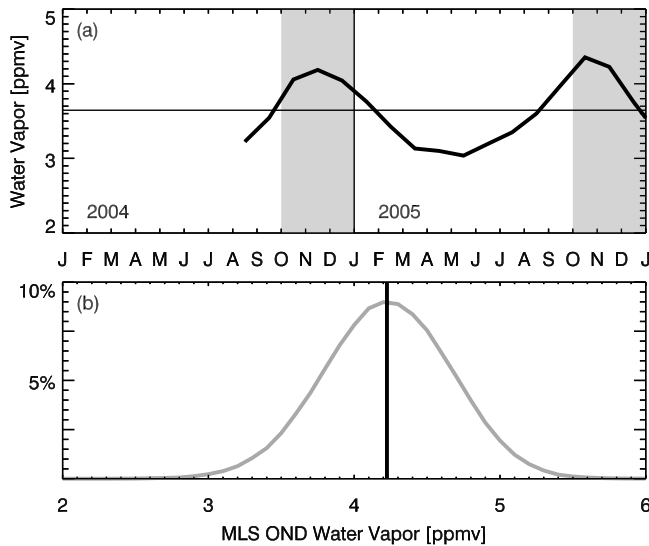
Figure 1. (a) Time series of Aura MLS water vapor at 68 hPa averaged over the tropics (15°S–15°N) for 2004–2005. Back trajectories are initialized during the grey shaded periods. (b) Mean (black vertical line) and distribution (grey line) of Aura MLS observations of water vapor at 68 hPa in the tropics for October through December of 2004 and 2005.

quently interpolated linearly in time and horizontal space to match the CLAUS resolution (3-hourly; 0.33° × 0.33°). For each tropical observation of CLAUS brightness temperature colder than 250 K, cloud top pressure is assigned as the highest pressure (lowest altitude) at which the CLAUS brightness temperature and the corresponding ERAI temperature profile are equal. The cloud top pressure is calculated using a linear interpolation in the natural logarithm of pressure when this temperature falls between two ERAI pressure levels.

[18] This procedure works well in cases for which there is a clear minimum in the temperature profile, such as the tropics; it fails, however, in cases for which the temperature profile in the UTLS is nearly isothermal, such as the mid-latitudes and polar regions. Poleward of 35° in each hemisphere, the ERAI temperature profile is adjusted prior to calculating cloud top pressure by averaging it with a moist adiabat calculated upward from 200 hPa. This approach is analogous to the 'semiadiabatic' profile used by *Sherwood et al.* [2004], and is intended to approximate the result of mixing between an overshooting convective turret and its environment. The primary consequence of the semiadiabatic adjustment is to eliminate the intersection of trajectories with convective events of unrealistic depth in midlatitudes (cloud tops well in excess of 400 K potential temperature [cf. *Dessler*, 2009]). The results we will discuss here focus on convection in regions between 10°N and 35°N, and are therefore not directly affected by the details or inclusion of this semiadiabatic adjustment. Indirect sensitivity within the results is limited to the calculation of the relative contribution of convection in the focus regions to the total global transport from convection.

2.4. Simulations of Water Vapor Transport

[19] Back trajectories are initialized during the annual water vapor maximum at 68 hPa in the tropics (October–

December; 15°S–15°N). Figure 1a shows the annual cycle of tropical mean water vapor at 68 hPa according to Aura MLS observations, along with the time periods during which trajectories are initialized (grey shading). The exact initialization points are determined by the time, nominal longitude and latitude, and potential temperature of Aura MLS observations of temperature within the tropics (15°S–15°N; ~600 daily). In practice these initialization criteria approximate a reverse domain filling technique, as MLS provides daily global coverage. Trajectories are integrated backwards in time for either 270 days (GMAO MERRA and ERAI) or until June 1 (NCEP/NCAR) regardless of initialization date. This ensures that the analysis encompasses the peak of summertime convective activity in the Southeast Asian monsoon region.

[20] Water vapor transport along each trajectory is simulated by advection-condensation: trajectories are assumed to detrain from convection at saturation and the mixing ratio at 68 hPa is assumed to be the minimum saturation mixing ratio encountered subsequent to detrainment [e.g., *Pierrehumbert and Roca*, 1998; *Fueglistaler et al.*, 2005; *Liu et al.*, 2010]. We refer to the location at which the minimum saturation mixing ratio occurs as the Lagrangian dry point (LDP). Trajectory uncertainties and intermediate mixing decouple the simulated water vapor at 68 hPa from contemporaneous MLS observations and preclude direct comparison between the two. Instead, the mean and distribution of water vapor observed by Aura MLS (shown in Figure 1b) is provided to establish an observational context for the simulated water vapor presented below.

[21] CLAUS observations of cloud top pressure are matched to trajectories using linear interpolation from the 0.33° × 0.33° CLAUS grid, and an intersection is considered to occur at the first point along the back trajectory for which trajectory pressure exceeds cloud top pressure. Cloud top brightness temperatures are nearly always colder than trajectory temperatures at the determined intersection points (95% of identified intersections), and the two temperatures generally agree to within 10 K (91% of identified intersections). This agreement suggests that the procedure for estimating cloud top pressure is reasonable, that the combination of different reanalysis temperature fields does not introduce a substantial bias, and that trajectories typically intersect deep convective clouds near the cloud top (where convective detrainment is maximum) rather than in the middle or at the base. Any intersection for which either cloud top or trajectory temperature is greater than 250 K (~300 hPa) is discarded as invalid, ensuring that only intersections within the typical detrainment zone for deep convection are considered [*Folkins et al.*, 2002].

3. Results

[22] Figure 2 presents the distribution within Southeast Asia of where trajectories intersect with thick high clouds according to both the NCEP/NCAR and GMAO MERRA trajectory ensembles. We identify three consistent primary source domains in both ensembles: the South Asian subcontinent and Bay of Bengal (referred to as MON and bounded by 70°E–105°E × 10°N–26°N), the South China and Philippine Seas (SCS; 105°E–150°E × 10°N–30°N), and the Tibetan Plateau and South Slope of the Himalayas
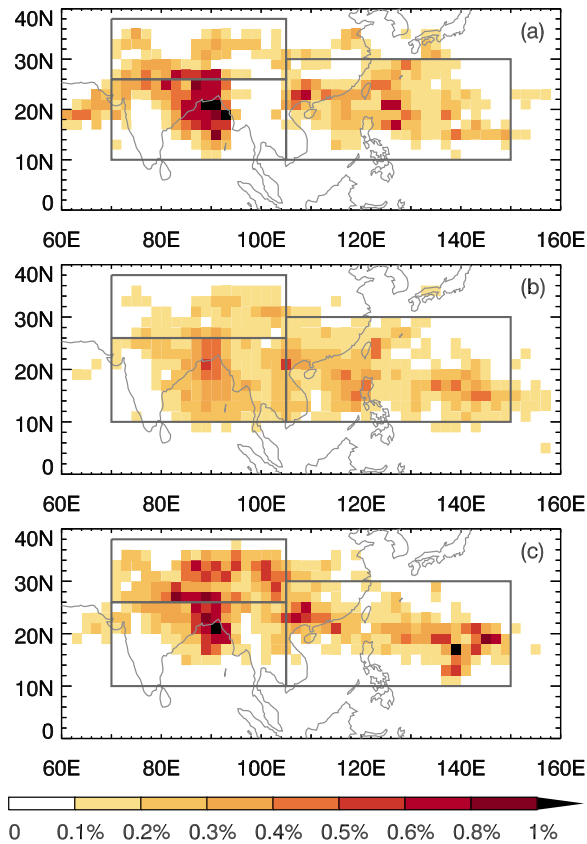
Figure 2. (a) Two-dimensional histogram of trajectory intersections with CLAUS observations of optically thick high clouds in the Southeast Asian monsoon region according to trajectories integrated using GMAO MERRA reanalysis, binned at 2° × 2°. (b) Same as Figure 2a but for trajectories integrated using ERA Interim reanalysis. (c) Same as Figure 2a but for trajectories integrated using NCEP/NCAR reanalysis. Boxes indicate the boundaries of the subregional convective source domains analyzed in this paper (see text for details).

Figure 3. (a) From bottom, fraction of summertime convective sources from SCS (orange), MON (blue), TIB (red), and all other locations (white) according to the GMAO trajectory ensemble. (b) Same as Figure 3a but for the ERAI trajectory ensemble. (c) Same as Figure 3a but for the NCEP trajectory ensemble.

the tropical stratosphere during boreal summer originates from convection over Southeast Asia, and all three convective source domains make substantial contributions to this flux.

[24] Figure 4 shows the mean circulation and temperature fields at 100 hPa during boreal summer over Southeast Asia, according to the GMAO MERRA reanalysis. The circulation is dominated by the Asian monsoon anticyclone, and the temperature field is characterized by a band of cold temperatures that arcs eastward from equatorial Africa, across the southern edge of the anticyclone, and south to the tropical western Pacific. Temperatures within this band are lowest just east of the Maritime Continent, in the region often referred to as the western Pacific 'cold trap' [e.g., *Holton and Gettelman*, 2001]. The prevailing conditions at 100 hPa are similar in the ERAI and NCEP/NCAR reanalyses. The arcing band of cold temperatures is observed in all three reanalyses with similar shape, although it is approximately 1 K warmer according to ERAI and 2 K

(TIB; 70°E–105°E × 26°N–35°N). These three source domains represent three geographically distinct convective regimes [e.g., *Hirose and Nakamura* 2005]. MON is a low-lying tropical domain predominantly characterized by large convective systems associated with the South Asian monsoon. SCS is a predominantly maritime domain characterized by medium to large convective systems. TIB is a mountainous, high altitude domain characterized by highly localized diurnal convective events.

[23] Combined, the MON, SCS, and TIB domains account for a large fraction of summertime convective sources identified globally (59% GMAO MERRA; 42% ERAI; 81% NCEP/NCAR), as shown in Figure 3. The three ensembles differ significantly in several respects throughout Figures 2 and 3. Most notably, the NCEP/NCAR ensemble indicates a greater global role for Southeast Asian convection as a whole, and for TIB convection in particular, than does the GMAO MERRA ensemble. Similarly, the GMAO MERRA ensemble indicates a greater role for Southeast Asian and TIB convection than does the ERAI ensemble. All three ensembles agree on a few fundamental characteristics, however: much of the flux of air from the troposphere into
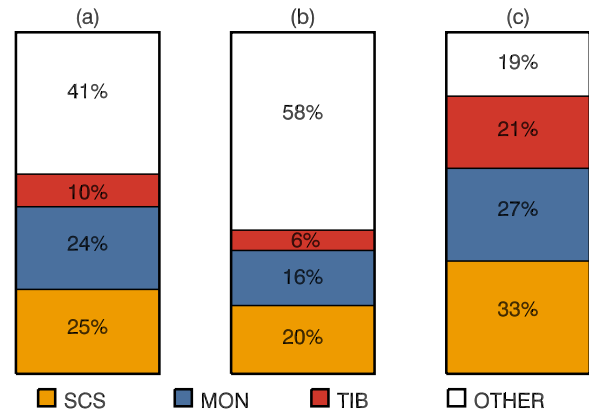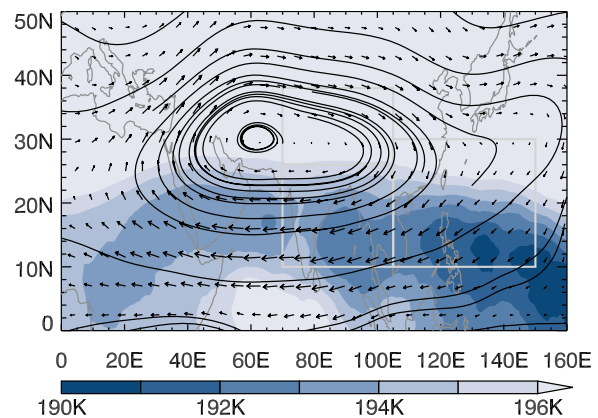

Figure 4. GMAO MERRA 100 hPa temperature (blue shaded contours) and winds (vectors) in the Southeast Asian region averaged over June, July, and August 2004 and 2005. Solid black curves show representative streamlines calculated from the wind field.
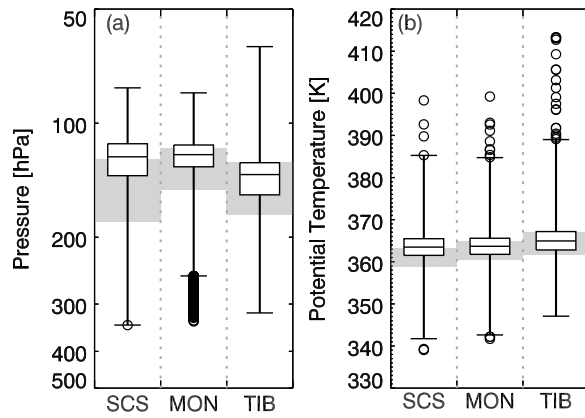
Figure 5. (a) Box and whisker plots of the pressure at which GMAO trajectories intersect with CLAUS observations of optically thick high clouds in the SCS, MON, and TIB subregional domains. Whiskers represent 5 times the interquartile range in the natural logarithm of pressure. Grey shading in each column represents the interquartile range of the level of zero net radiative heating (LZRH) for each region during boreal summers 2004 and 2005 according to the GMAO MERRA reanalysis. (b) Same as Figure 5a but for the potential temperature at which the intersections occur.

warmer according to NCEP/NCAR. The monsoon anticyclone exhibits slight variations in shape (ERAI indicates a more symmetric oval than does GMAO MERRA, and NCEP/NCAR a pronounced kidney shape with the dimple at the northern edge at 70°E), but its location and its spatial relationship to the three source domains is consistent among these three data sets.

[25] Figure 5 details the properties of intersections between trajectories and CLAUS observations of convection in the three subregional domains. More than half of the intersections in each domain occur between 200 hPa and 100 hPa, and most occur at or above the typical level of zero radiative heating (LZRH). As described in the introduction, the LZRH is the boundary between radiative subsidence (below), and radiative ascent (above). The results presented in Figure 5 suggest a picture in which stratospheric air generally traces back to convective detrainment within the TTL, with occasional direct convective injection into the lower stratosphere and occasional transport into the TTL from detrainment below. This picture is broadly consistent with current understanding [*Fueglistaler et al.*, 2009a; *Schiller et al.*, 2009; *Steinwagner et al.*, 2010].

[26] Using pressure as the vertical coordinate, as in Figure 5a, the median intersection with MON convective events occurs highest of the three domains, followed by SCS, and with TIB the shallowest; however, a different picture emerges when potential temperature is used as the vertical coordinate, as in Figure 5b. In the latter case, intersections with TIB convective events occur highest, followed by MON, and with SCS shallowest. This shift is the result of the downward slope of isentropes above 350 K when moving from the deep tropics into the extratropics, and may be of particular relevance for transport into the stratosphere from TIB convection. For the central and eastern portions of TIB, where the convective sources are concentrated according to

Figure 2, the monsoon anticyclone pushes air southward toward MON (Figure 4). The prevailing initial isentropic motion for air detrained from TIB convection is therefore upward, likely supplementing radiative ascent. Furthermore, as the LZRH is typically located at lower potential temperatures over MON (Figure 5), these prevailing conditions may allow air detrained from TIB convection to isentropically cross the LZRH into the layer of radiative ascent following detrainment. We will return to these points later.

[27] Figure 6 summarizes the character of water vapor transport to 68 hPa from each subregional domain according to the advection-condensation simulations. It is dangerous to overinterpret the absolute values of water vapor transport produced by the advection-condensation simulation, as highlighted both by the disparity between these three trajectory ensembles and by the analysis of *Liu et al.* [2010]; rather, we will focus on the relative differences among the three subregional convective source domains, and particularly areas of consistency in the three ensembles. Trajectories from TIB are typically moistest, followed by MON trajectories, and with SCS trajectories the driest. These relative differences in simulated water vapor are consistent in all trajectory ensembles, and are observed in both the mean and the distribution. In particular, TIB trajectories are most likely to be anomalously moist and least likely to be anomalously dry, while SCS trajectories are least likely to be anomalously moist and most likely to be anomalously dry, with MON trajectories in between.

[28] Some additional qualitative insight can be gained by comparing and contrasting the simulated means and distributions to the mean and distribution of water vapor at 68 hPa observed by Aura MLS (Figure 1b). With the exception of NCEP/NCAR, the simulated water vapor values are
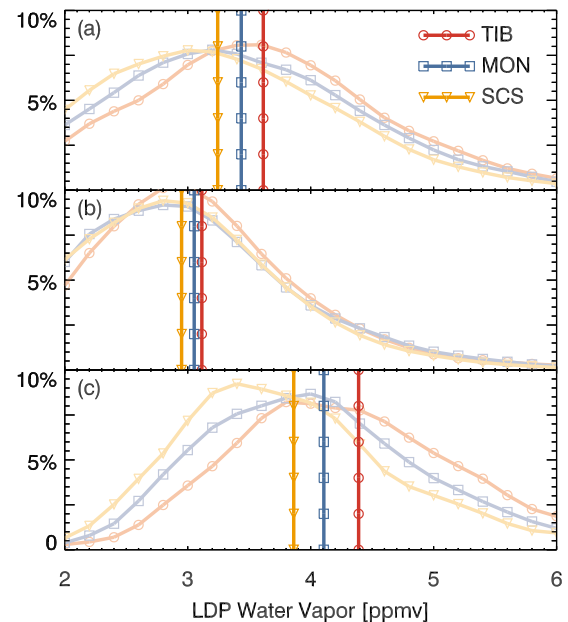

Figure 6. (a) Mean (bold vertical lines) and distribution (faded lines) of LDP water vapor for GMAO MERRA trajectories with convective sources in SCS (orange triangles), MON (blue squares), and TIB (red circles). (b) Same as Figure 6a but for ERA Interim trajectories. (c) Same as Figure 6a but for NCEP/NCAR trajectories.
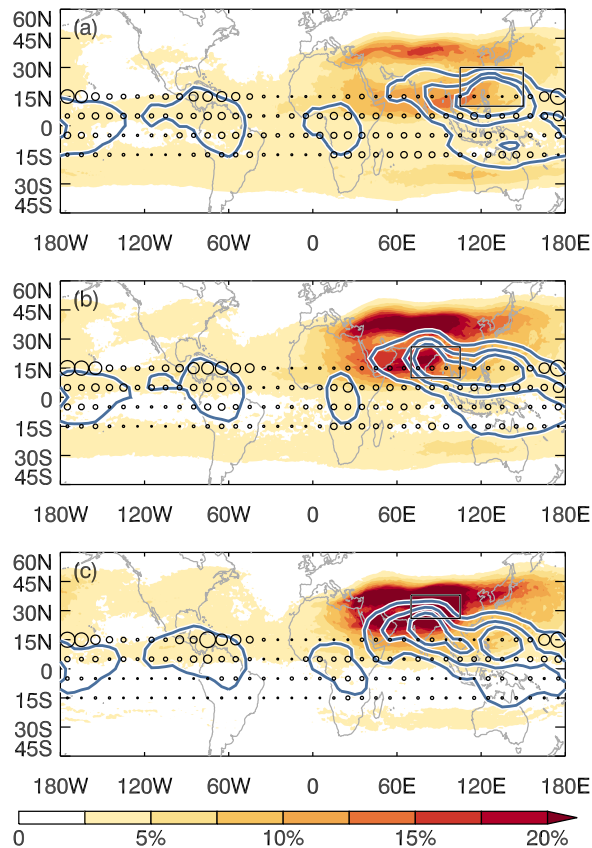
Figure 7. Preferred transport pathways (shading), distributions of LDP locations (solid blue contours), and distribution of entry to the tropical pipe (above 75 hPa; within 15°S–15°N) (black circles) for GMAO MERRA trajectories with convective sources in (a) SCS, (b) MON, and (c) TIB.

considerably drier than all but a small fraction of the observed values, which suggests that neglected processes may be important. Such processes might include supersaturation with respect to ice, condensate reevaporation, or an enhanced role of direct injection by convection penetrating the tropopause. A detailed examination of these is outside of the scope of the present study, and will be presented in future work. The observed distribution is also much narrower than the simulated distributions. This feature is consistent with expectations: mixing above the cold point between particularly moist and particularly dry trajectories will tend to compress the distribution toward the mean.

[29] The underlying causes of the systematic differences in simulated water vapor transport observed in Figure 6 can be deduced by examining the characteristics of transport from each domain, which are presented for the GMAO MERRA ensemble in Figure 7. The shaded contours in Figure 7 show the density of transport pathways between deep convection in each of the three subregional domains identified above and 68 hPa in the tropics, collapsed into a horizontal plane. This metric is calculated by determining the fraction of trajectories from the specified domain that sample a given $1° \times 1°$ gridded column at least once between convective detrainment and 68 hPa in the tropics. Figure 7 also shows two additional metrics of transport characteristics: the distribution of where trajectories

encounter their LDPs (solid blue contours), and the distribution of where trajectories enter the tropical pipe (black circles). This latter metric is calculated in $10° \times 10°$ bins as the number of trajectories within the ensemble that cross into the volume above 75 hPa and between 15°S and 15°N, and is normalized so that the maximum entry location has a radius of 1.

[30] Transport pathways from all three domains are dominated to varying degrees by the Asian monsoon anticyclone. TIB trajectories are confined very tightly to the anticyclone, MON trajectories are confined somewhat more loosely, and SCS trajectories are confined still more loosely. The reasons for these differences are apparent in the circulation characteristics of the monsoon anticyclone (shown in Figure 4), particularly the streamlines that pass through each domain. The central core of the anticyclone is located near 30°N and 60°E. TIB convection detrains nearby to this central core, where streamlines spiral tightly around the anticyclone. MON convection detrains slightly farther away from the central core, where the streamlines begin to spiral more noticeably outward. SCS convection detrains near the edge of the anticyclone, where the streamlines are much more loosely associated with the anticyclone.

[31] Further differences in the transport from the three domains are apparent in the distributions of LDP locations. The center of the LDP distribution is shifted north and west for MON trajectories relative to SCS trajectories, and is shifted still further north and west for TIB trajectories. Shifts of this distribution to the north and west indicate a reduction in the relative influence of the very cold temperatures in the tropopause layer over the western Pacific (Figure 4) [see also *Newell and Gould-Stewart*, 1981; *Holton and Gettelman*, 2001; *Fueglistaler et al.*, 2005], and limit the extent of the imprint of these temperatures on water vapor reaching 68 hPa in the tropics. This shift is more readily apparent in Figure 8, which directly contrasts the spatial distributions of LDPs for TIB and MON trajectories. The column mean LDP water vapor is plotted as shaded cells for each trajectory ensemble. Figure 8 shows that TIB LDPs are shifted northward and westward toward warmer, moister values relative to MON LDPs. This shift is observed in all three trajectory ensembles, although it is most pronounced in NCEP/NCAR and least pronounced in ERAI, as implied by the discrepancies between ensembles in Figure 6.

[32] Figure 7 indicates that trajectories are preferentially ejected from the anticyclone at two locations, to the northeast (upper right corner of Figure 4), and to the southwest (lower left corner of Figure 4). Trajectories ejected to the northeast are predominantly swept into the tropical pipe between 160°E and 160°W. A lower-altitude analogue of this transport pathway into the tropics can be seen in Figure 4 as the pair of streamlines that cut into the tropics at the lower right-hand corner. Figure 4 indicates that air following this pathway passes directly through the western Pacific cold trap.

[33] At this point we revisit the idea that air detrained from TIB convection receives a 'head start' by being detrained onto higher isentropic surfaces (Figure 5). When combined with the tighter confinement of TIB trajectories to the central core of the anticyclone, this suggests that TIB trajectories may typically peel off from the anticyclone higher than MON or SCS trajectories, presuming similar rates of ascent. The distribution of trajectory entry to the
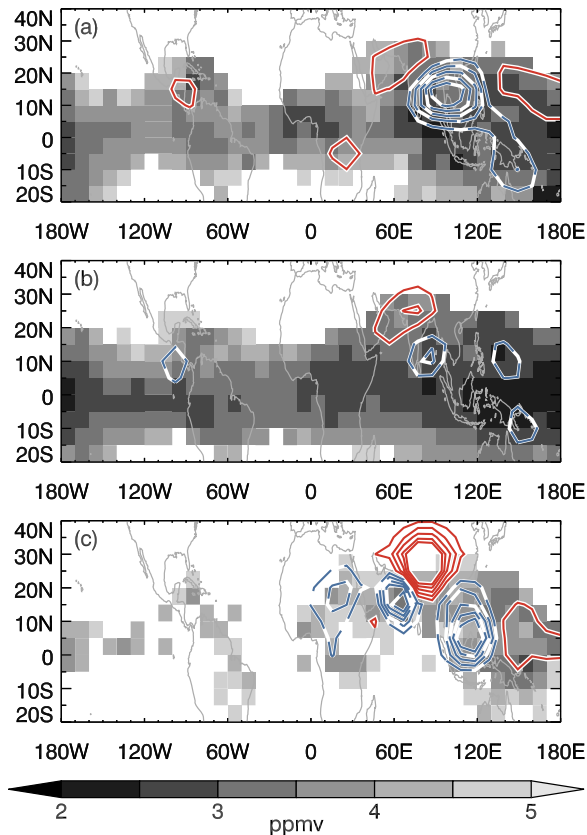
Figure 8. (a) Difference between the horizontal distributions of LDP locations for the TIB and MON trajectory ensembles according to GMAO MERRA. Solid red contours indicate a greater density of TIB LDPs; dashed blue contours indicate a greater density of MON LDPs. Shading indicates column mean LDP water vapor amounts. (b) Same as Figure 8a but for ERA Interim. (c) Same as Figure 8a but for NCEP/NCAR. Contour interval is 0.5 times a reasonable contour interval for the absolute distributions.

tropical pipe (black circles in Figure 7) supports this picture. TIB trajectories are more likely to first enter the tropical pipe above 75 hPa by crossing the northern boundary than MON or SCS trajectories, while SCS and MON trajectories are more likely to enter from below, through the TTL, than TIB trajectories. This difference suggests that SCS and MON trajectories are more likely to experience slow ascent while meandering through the tropics, where tropopause layer temperatures are coldest, while TIB trajectories are more likely to predominantly experience slow ascent within the monsoon anticyclone.

[34] Further evidence is presented in Figure 9, which directly contrasts the global zonal mean distributions of LDPs for TIB and MON trajectories. TIB LDPs are shifted upward and northward toward warmer, moister values relative to MON LDPs. The upward shift is particularly pronounced in the tropics, where we expect any additional lift gained in the monsoon anticyclone to be particularly effective at enabling the trajectories to bypass the western Pacific cold trap (recall that trajectories from all three domains preferentially enter the tropics between 160°E and

160°W, so that the cold trap appears to be laid for all three). This upward shift of LDP location, together with the northward and westward shifts detailed above, provides a reasonable and physically consistent qualitative explanation for the differences between the distributions shown in Figure 6, particularly the systematic differences in the likelihoods of especially moist and especially dry trajectories.

[35] For the sake of brevity and clarity, we have only presented results for the GMAO MERRA ensemble in Figure 7. Although there are some quantitative differences between the three ensembles, the qualitative results that we have focused on above are wholly consistent. The most important difference is the localization of the LDP distributions, which are relatively more distinct according NCEP/NCAR and relatively less distinct according to ERAI, as is readily apparent in Figure 8. The predominant pathways are remarkably similar among the three data sets, particularly with respect to the points we have raised: SCS trajectories are loosely confined to the edge of the anticyclone, MON trajectories are more tightly confined within the anticyclone, and TIB trajectories are most tightly confined to the center of the anticyclone. There are some discrepancies in the meridional location of preferred entry to the tropical pipe; however, all three ensembles indicate substantial entry between 160°E and 160°W, and all three ensembles indicate that TIB trajectories are more likely then MON or SCS trajectories to enter the tropical pipe on the northern edge, while
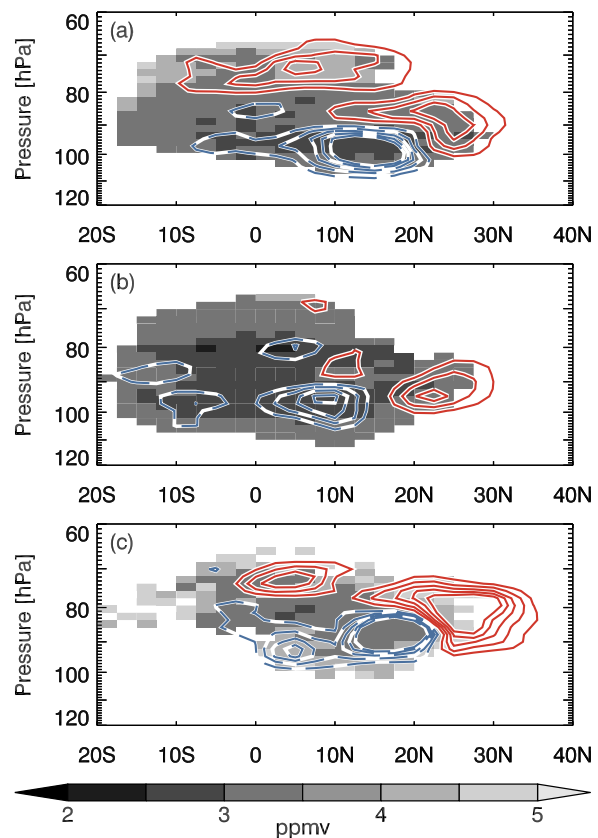

Figure 9. Same as Figure 8 but for global zonal mean differences in LDP distributions and water vapor amounts.
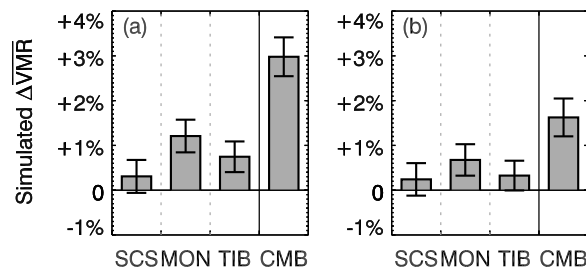
Figure 10. (a) Contributions of trajectories from SCS, MON, TIB, and the combination of the three domains (CMB) to the mean simulated water vapor at 68 hPa during October through December 2004 and 2005 according to GMAO MERRA. (b) Same as Figure 10a but for ERA Interim. Error bars encompass twice the standard error of the mean.

trajectories from MON and SCS are more likely than those from TIB to enter from below.

[36] Now we turn to the broader picture: having established that there are systematic differences in water vapor transport from different convective regimes within Southeast Asia, we should estimate the impact of these systematic differences on tropical mean stratospheric water vapor. Figure 10 shows the difference in the mean simulated water vapor at 68 hPa in the tropics that is effected by excluding the trajectories that emanate from summertime convection in each subregional domain. The values are plotted on a reverse scale so that a moistening influence on the mean flux (i.e., a decrease in the mean simulated water vapor transport when the trajectory subset is excluded) is shown as positive, whereas a drying influence is shown as negative. Here, we neglect the fraction of trajectories that do not intersect with convection during the analysis period. This amounts to an assumption that the mean water vapor at 68 hPa is determined solely by transport from convection within the previous nine months, or equivalently that the trajectories for which no convective source has been identified do not have radically different characteristics than those for which one has. Therefore, results are only shown for GMAO MERRA and ERAI in Figure 10, as these are the ensembles for which we have identified convective sources for a substantial fraction of the initialized trajectories (66% of GMAO MERRA; 80% of ERAI).

[37] Removing the contribution of any one of the three Southeast Asian subregional convective source domains has only a minor influence on mean water vapor at 68 hPa, with changes on the order of 1% (~0.05 ppmv) or less. In particular, the relatively high water vapor transport along TIB trajectories (Figure 6) is effectively offset by the relatively small fraction of trajectories emanating from TIB (Figure 3): TIB exerts a net moistening influence, but it is likely less than 1% in the mean. Both ensembles indicate that, of the three Southeast Asian subregional domains, MON exerts the strongest influence, with a net moistening of around 1%, just as both ensembles suggest that trajectories from SCS are quite similar to the average of all trajectories. Eliminating the combined contribution of SCS, MON, and TIB dries the simulated mean water vapor at 68 hPa by approximately 3%

(0.1 ppmv) in the GMAO MERRA ensemble and approximately 2% (0.05 ppmv) in the ERAI ensemble.

4. Discussion

[38] We will next identify some limitations and caveats of the method, so that the results may be more easily placed into proper context. One obvious limitation that is implicit in the Lagrangian trajectory approach used here is uncertainties in trajectory positions, particularly at such long integrations (here, up to 270 days). The implications of this uncertainty for the subset of trajectories that we have studied in detail can be roughly estimated by comparing and contrasting the results of the three trajectory ensembles, which rely on three independent underlying global models and assimilation systems. As noted above, the details of the three ensembles differ, but the qualitative conclusions are robust. In particular, all three ensembles identify the same three subregional domains within Southeast Asia, all three ensembles simulate similar systematic differences in water vapor transport to 68 hPa, and in all three ensembles these differences in water vapor transport can be directly related to similar qualitative differences in bulk transport characteristics.

[39] A second and potentially more important limitation concerns the representation of convection. Using the CLAUS observations is a step toward greater realism and reduced sensitivity to details of the underlying reanalysis model relative to previous techniques (such as evaluating where trajectories cross a given isobaric or isentropic surface), but the calculated cloud top heights may still be unrealistically low. *Sherwood et al.* [2004] and *Minnis et al.* [2008] reported that estimates of deep convective cloud top heights derived from IR brightness temperatures (such as CLAUS) are generally biased low relative to observations of cloud top heights obtained using Lidar instruments, and suggested reasonable corrections. Applying such bias corrections acts to enhance the importance of direct convective injection beyond the tropopause into the stratosphere. As indicated by Figure 5, the trajectories presented above generally experience detrainment from convection within the tropopause layer followed by slow ascent into the tropical stratosphere; convective events that penetrate the tropical tropopause (~380 K) are infrequent. Recent observational studies suggest that detrainment in the tropopause layer followed by slow ascent accurately describes most air entering the tropical stratosphere, but there is evidence that convective injection directly into the stratosphere may play an important secondary role beyond that indicated by our results [*Read et al.*, 2004; *Corti et al.*, 2008; *Schiller et al.*, 2009; *Steinwagner et al.*, 2010]. Accordingly, our results may be viewed as robust with respect to the transport of water vapor from Southeast Asia through the tropopause layer and into the stratosphere, with the influence of direct convective injection yet to be explored.

[40] One final limitation that merits mention is the limited overlap between observational data sets. The CLAUS data set covers the period between July 1983 and June 2006, while Aura MLS has been operational from August 2004 to the present. Several other recently launched satellite instruments could be valuable for either extending the scope of this study or for validating estimates of cloud top height using CLAUS. The CLAUS data set is particularly useful

because it provides global coverage at high resolution in both space (0.33°) and time (3 h). The continuing availability of this data set or one like it would be particularly valuable, and should be a high priority for continuing study of the atmospheric hydrologic cycle.

[41] We now return to the scientific debate summarized at the end of section 1. To recap, *Fu et al.* [2006] showed that convection over the Tibetan Plateau and South Slope introduces substantial amounts of water vapor to the local lower stratosphere, and suggested that transport from this region could bypass the tropical tropopause cold trap and represent a significant moisture source to the tropical stratosphere. Results using global climate models supported this hypothesis, indicating that deep convective events over Southeast Asia, and particularly over the Tibetan Plateau, are highly influential in setting the amplitude of the moist phase of the tropical tape recorder [*Bannister et al.*, 2004; *Lelieveld et al.*, 2007]. Other studies found that the influence of deep convection over the Tibetan Plateau is minor, however, and suggested that the most influential convective sources within Southeast Asia are located over the Bay of Bengal and South China Sea [*Park et al.*, 2007; *James et al.*, 2008; *Devasthale and Fueglistaler*, 2010].

[42] The results presented in section 3 provide valuable context to this debate. According to these results, convection over Southeast Asia does represent a prominent source of air to the moist phase of the tape recorder during boreal summer (Figure 3). The largest convective sources within Southeast Asia are located over the Bay of Bengal and South China Sea; however, convection over the Tibetan Plateau and South Slope of the Himalayas also plays a significant role (Figures 2 and 3). Transport from convection over the Tibetan Plateau and South Slope is systematically moister than transport from the Bay of Bengal or South China Sea (Figure 6), because the typical pathway from this source domain preferentially avoids the coldest tropical tropopause temperatures and bypasses the western Pacific cold trap (Figures 2–8). The overall effect of this bypass mechanism on stratospheric water vapor appears to be small, however, when placed in the broader context of global water vapor flux into the tropical stratosphere (Figure 10).

[43] These conclusions highlight several pitfalls intrinsic to examining the transport of water vapor from the troposphere into the tropical stratosphere. This transport process represents the synthesis of local convective events with large-scale advection, and occurs within a complex four-dimensional temperature field. It is therefore difficult, and perhaps dangerous, to attempt to comprehend the whole according to its parts. For instance, one might reasonably presume from Figures 6–9 that deep convection over the Tibetan Plateau and South Slope of the Himalayas could be a determining influence on the seasonal maximum of tropical stratospheric water vapor. Similarly, one might conclude solely from the distribution of deep convection within Southeast Asia that deep convection over TIB is entirely negligible as a source of tropical stratospheric water vapor. The contextual information provided when the distribution of deep convection is combined with the transport characteristics and temperature field shows that reality lies between these two divergent conclusions. Transport from deep convection over TIB into the tropical stratosphere provides a mechanism by which particularly moist air can bypass the coldest tropopause temperatures; however, the distribution of deep convection within Southeast Asia limits the overall impact of this mechanism.

[44] Finally, we note that interest in the contributions of convective sources within Southeast Asia to water vapor in the tropical stratosphere has been motivated in large part by efforts to properly characterize the processes that control the annual water vapor maximum in the stratosphere [e.g., *Fu et al.*, 2006; *Lelieveld et al.*, 2007]. In particular, do changes in tropical tropopause temperature suffice to explain the magnitude of the moist phase of the water vapor tape recorder, or do changes in the distribution of convection also play a substantial role? These results may be used to provide an additional point of reference to this question. As noted in the discussion of Figure 10 above, eliminating the combined fluxes of water vapor from SCS, MON, and TIB dries the simulated seasonal maximum by 0.1 ppmv according to the GMAO MERRA trajectory ensemble, and by 0.05 ppmv according to ERAI. The observed amplitude of the annual cycle of water vapor at 68 hPa from 2004 to 2009 is 1.22 ppmv according to MLS, with the tropical mean from October through December taken as the annual maximum and the tropical mean from April through June as the minimum. At first glance, this suggests that the northward shift of convection associated with the Southeast Asian monsoon may be responsible for order 5% (8% GMAO MERRA; 4% ERAI) of the seasonal change; however, *Liu et al.* [2010] showed that just as simulated water vapor is reduced relative to observed, the amplitude of the simulated seasonal cycle is reduced (i.e., the dry bias of the simulations relative to observations is largest at the annual maximum and smallest at the annual minimum). Normalizing by the ratio of simulated mean water vapor (3.2 ppmv GMAO MERRA; 2.9 ppmv ERAI) to observed (4.2 ppmv MLS), the estimated amplitude of the seasonal cycle is approximately 0.9 ppmv for GMAO MERRA and 0.8 ppmv for ERAI, suggesting that Southeast Asia may contribute up to order 10% (11% GMAO MERRA; 6% ERAI) of the seasonal change. Accordingly we conjecture that only a few percent of the magnitude of the moist phase of the tropical tape recorder may be related to the flux of water vapor from summertime convection over Southeast Asia.

5. Summary and Conclusions

[45] Convection within Southeast Asia is shown to be a significant source of water vapor to the tropical stratosphere during the annual water vapor maximum. Summertime convective sources within Southeast Asia are concentrated in three geographically distinct subregional domains: the South Asian subcontinent and Bay of Bengal (MON), the South China and Philippine Seas (SCS), and the Tibetan Plateau and South Slope of the Himalayas (TIB). Systematic differences in the character of transport pathways from these three domains lead to systematic differences in the flux of water vapor into the tropical stratosphere.

[46] Trajectories emanating from SCS convection generally follow along the edge of the Asian monsoon anticyclone before spinning off into the tropics. These trajectories frequently pass through the western Pacific cold trap, and are consequently characterized by both a high fraction of particularly dry transport and a low fraction of particularly

moist transport. MON trajectories are also transported largely within the Asian monsoon anticyclone, but are confined more tightly to the central core of the anticyclone than SCS trajectories. MON trajectories are less likely than SCS trajectories to sample LDPs within the western Pacific cold trap, and are more likely to sample LDPs within the relatively warmer temperatures at the southern edge of the monsoon anticyclone. Consequently, transport by MON trajectories is typically moister than transport by SCS trajectories. TIB trajectories are confined even more tightly to the monsoon anticyclone than MON trajectories. The LDPs of trajectories from TIB are generally shifted northwestward and upward, toward warmer temperatures and higher saturation mixing ratios, relative to MON and SCS LDPs.

[47] The systematic differences in water vapor transport from the three convective source domains have substantial impacts upon the total flux of water vapor from Southeast Asia to the tropical lower stratosphere. In the broader context of tropical mean lower stratospheric water vapor, however, these impacts appear to be small: the total flux of water vapor from Southeast Asia is estimated to be responsible for only a few percent of the amplitude of the seasonal cycle. Based on these results, it appears unlikely that shifts in the distribution of convective sources are crucial for explaining seasonal changes of stratospheric water vapor. It is important to keep in mind that this analysis has only considered water vapor, and that regional differences in water vapor transport are strongly smoothed by the dependence of water vapor on the temperature field. The distribution of convective source regimes and differences between them may have much larger implications for other chemical species, such as very short-lived bromine compounds [*Sinnhuber and Folkins*, 2006; *Levine et al.*, 2007], or hydrogen cyanide [*Pumphrey et al.*, 2008; *Randel et al.*, 2010].

[48] Several limitations inherent to the experimental methodology have been identified, and their implications for the results have been discussed. It is concluded that the results are robust in the limiting case for which air in the stratosphere has experienced detrainment from convection within the TTL followed by slow ascent. Recent observational studies suggest that this limiting case accurately describes most air entering the tropical stratosphere [*Read et al.*, 2004; *Schiller et al.*, 2009; *Steinwagner et al.*, 2010], although the relative role of direct convective injection into the stratosphere remains uncertain [*Corti et al.*, 2008; *Steinwagner et al.*, 2010]. This role will be examined in detail in an ongoing follow-up study.

References

Bannister, R. N., A. O'Neill, A. R. Gregory, and K. M. Nissen (2004), The role of the south-east Asian monsoon and other seasonal features in creating the 'tape-recorder' signal in the Unified Model, *Q. J. R. Meteorol. Soc.*, 130, 1531–1554, doi:10.1256/qj.03.106.

Bosilovich, M. (2008), NASA's Modern Era Retrospective-analysis for Research and Applications: Integrating Earth observations [online], *Earthzine*, http://www.earthzine.org/2008/09/26/nasas-modern-era-retrospective-analysis/.

Corti, T., et al. (2008), Unprecedented evidence for overshooting convection hydrating the tropical stratosphere, *Geophys. Res. Lett.*, 35, L10810, doi:10.1029/2008GL033641.

Dessler, A. E. (2009), Clouds and water vapor in the Northern Hemisphere summertime stratosphere, *J. Geophys. Res.*, 114, D00H09, doi:10.1029/2009JD012075.

Devasthale, A., and S. Fueglistaler (2010), A climatological perspective of deep convection penetrating the TTL during the Indian summer monsoon from the AVHRR and MODIS instruments, *Atmos. Chem. Phys.*, 10, 4573–4582.

Dvortsov, V. L., and S. Solomon (2001), Response of the stratospheric temperatures and ozone to past and future increases in stratospheric humidity, *J. Geophys. Res.*, 106(D7), 7505–7514, doi:10.1029/2000JD900637.

Folkins, I., K. K. Kelly, and E. M. Weinstock (2002), A simple explanation for the increase in relative humidity between 11 and 14 km in the tropics, *J. Geophys. Res.*, 107(D23), 4736, doi:10.1029/2002JD002185.

Forster, P. M. D. F., and K. P. Shine (2002), Assessing the climate impact of trends in stratospheric water vapor, *Geophys. Res. Lett.*, 29(6), 1086, doi:10.1029/2001GL013909.

Fu, R., et al. (2006), Convective transport over the Tibetan Plateau—A short-circuit of water vapor and polluted air to the global stratosphere, *Proc. Natl. Acad. Sci. U. S. A.*, 103, 5664–5669, doi:10.1073/pnas.0601584103.

Fueglistaler, S., M. Bonazzola, P. H. Haynes, and T. Peter (2005), Stratospheric water vapor predicted from the Lagrangian history of air entering the stratosphere in the tropics, *J. Geophys. Res.*, 110, D08107, doi:10.1029/2004JD005516.

Fueglistaler, S., A. E. Dessler, T. J. Dunkerton, I. Folkins, Q. Fu, and P. W. Mote (2009a), Tropical tropopause layer, *Rev. Geophys.*, 47, RG1004, doi:10.1029/2008RG000267.

Fueglistaler, S., B. Legras, A. Beljaars, J.-J. Morcrette, A. Simmons, A. M. Tompkins, and S. Uppala (2009b), The diabatic heat budget of the upper troposphere and lower/mid stratosphere in ECMWF reanalyses, *Q. J. R. Meteorol. Soc.*, 135, 21–37, doi:10.1002/qj.361.

Fujinami, H., S. Nomura, and T. Yasunari (2005), Characteristics of diurnal variations in convection and precipitation over the southern Tibetan Plateau during summer, *SOLA*, 1, 49–52, doi:10.2151/sola.2005-014.

Hirose, M., and K. Nakamura (2005), Spatial and diurnal variations of precipitation systems over Asia observed by the TRMM Precipitation Radar, *J. Geophys. Res.*, 110, D05106, doi:10.1029/2004JD004815.

Hodges, K., D. W. Chappell, G. J. Robinson, and G. Yang (2000), An improved algorithm for generating global window brightness temperatures from multiple satellite infrared imagery, *J. Atmos. Oceanic Technol.*, 17, 1296–1312.

Holton, J. R., and A. Gettelman (2001), Horizontal transport and the dehydration of the stratosphere, *Geophys. Res. Lett.*, 28, 2799–2802.

James, R., M. Bonazzola, B. Legras, K. Surbled, and S. Fueglistaler (2008), Water vapor transport and dehydration above convective outflow during Asian monsoon, *Geophys. Res. Lett.*, 35, L20810, doi:10.1029/2008GL035441.

Kalnay, E., et al. (1996), The NCEP/NCAR 50-year reanalysis project, *Bull. Am. Meteorol. Soc.*, 79, 437–471.

Lambert, A., et al. (2007), Validation of the Aura Microwave Limb Sounder middle atmosphere water vapor and nitrous oxide measurements, *J. Geophys. Res.*, 112, D24S36, doi:10.1029/2007JD008724.

Lelieveld, J., et al. (2007), Stratospheric dryness: model simulations and satellite observations, *Atmos. Chem. Phys.*, 7, 1313–1332.

Levine, J. G., P. Braesicke, N. R. P. Harris, N. H. Saage, and J. A. Pyle (2007), Pathways and timescales for troposphere-to-stratosphere transport via the tropical tropopause layer and their relevance for very short lived substances, *J. Geophys. Res.*, 112, D04308, doi:10.1029/2005JD006940.

Liu, L., J. Feng, R. Chu, Y. Zhou, and K. Ueno (2002), The diurnal variation of precipitation in the monsoon season in the Tibetan Plateau, *Adv. Atmos. Sci.*, 19(2), 365–378.

Liu, Y., S. Fueglistaler, and P. H. Haynes (2010), The advection-condensation paradigm for stratospheric water vapor, *J. Geophys. Res.*, 115, D24307, doi:10.1029/2010JD014352.

Livesey, N. J., et al. (2007), EOS Aura Microwave Limb Sounder version 2.2 level 2 data quality and description document, *Tech. Rep. JPL D-33509*, 115 pp., Jet Propul. Lab., Pasadena, Calif.

Lucchesi, R. (2008), File specification for MERRA products, report, NASA Global Modeling and Assim. Off., Greenbelt, Md. (available at http://gmao.gsfc.nasa.gov/research/merra/MERRA_FileSpec_DRAFT_09_02_2008.pdf.)

Minnis, P., C. R. Yost, S. Sun-Mack, and Y. Chen (2008), Estimating the top altitude of optically thick ice clouds from thermal infrared satellite observations using CALIPSO data, *Geophys. Res. Lett.*, *35*, L12801, doi:10.1029/2008GL033947.

Mote, P. W., et al. (1996), An atmospheric tape-recorder: the imprint of tropical tropopause temperatures on stratospheric water vapor, *J. Geophys. Res.*, *101*, 3989–4006.

Moyer, E. J., F. W. Irion, Y. L. Yung, and M. R. Gunson (1996), ATMOS stratospheric deuterated water and implications for troposphere-stratosphere transport, *Geophys. Res. Lett.*, *23*, 2385–2388, doi:10.1029/96GL01489.

Newell, R. E., and S. Gould-Stewart (1981), A stratospheric fountain?, *J. Atmos. Sci.*, *38*, 2789–2796.

Park, M., W. J. Randel, A. Gettelman, S. T. Massie, and J. H. Jiang (2007), Transport above the Asian summer monsoon anticyclone inferred from Aura Microwave Limb Sounder tracers, *J. Geophys. Res.*, *112*, D16309, doi:10.1029/2006JD008294.

Petersen, W. A., and S. A. Rutledge (2001), Regional variability in tropical convection: Observations from TRMM, *J. Clim.*, *14*, 3566–3586.

Pierrehumbert, R. T., and R. Roca (1998), Evidence for control of Atlantic subtropical humidity by large scale advection, *Geophys. Res. Lett.*, *25*, 4537–4540, doi:10.1029/1998GL900203.

Pumphrey, H. C., C. Boone, K. A. Walker, P. Bernath, and N. J. Livesey (2008), Tropical tape recorder observed in HCN, *Geophys. Res. Lett.*, *35*, L05801, doi:10.1029/2007GL032137.

Randel, W. J., M. Park, L. Emmons, D. Kinnison, P. Bernath, K. A. Walker, C. Boone, and H. Pumphrey (2010), Asian monsoon transport of pollution to the stratosphere, *Science*, *328*(5978), 611–613, doi:10.1126/science.1182274.

Read, W. G., D. L. Wu, J. W. Waters, and H. C. Pumphrey (2004), Dehydration in the tropical tropopause layer: Implications from the UARS Microwave Limb Sounder, *J. Geophys. Res.*, *109*, D06110, doi:10.1029/2003JD004056.

Rienecker, M. M., et al. (2008), The GEOS-5 data assimilation system - Documentation of versions 5.0.1, 5.1.0, and 5.2.0., *Tech. Rep. NASA/TM*-2008-104606, 101 pp., NASA Goddard Space Flight Cent., Greenbelt, Md.

Robinson, G. J., and K. Hodges (2005), CLAUS: CLoud Archive User Service user guide version 1.4, report, NERC Environ. Syst. Serv. Cent., Reading, U. K. (Available at http://badc.nerc.ac.uk/data/claus/userguide.pdf.)

Schiller, C., J. U. Grooß, P. Konopka, F. Plöger, F. H. Silva dos Santos, and N. Spelten (2009), Hydration and dehydration at the tropical tropopause, *Atmos. Chem. Phys.*, *9*, 9647–9660.

Schoeberl, M. R., and L. Sparling (1995), Trajectory modeling, in *Diagnostic Tools in Atmospheric Physics: Proceedings of the International School of Physics Enrico Fermi*, vol. 124, edited by G. Fiocco and G. Visconti, pp. 289–306, IOS Press, Amsterdam.

Schwartz, M. J., et al. (2008), Validation of the Aura Microwave Limb Sounder temperature and geopotential height measurements, *J. Geophys. Res.*, *113*, D15S11, doi:10.1029/2007JD008783.

Sherwood, S. C., J.-H. Chae, P. Minnis, and M. McGill (2004), Underestimation of deep convective cloud tops by thermal imagery, *Geophys. Res. Lett.*, *31*, L11102, doi:10.1029/2004GL019699.

Shindell, D. T. (2001), Climate and ozone response to increased stratospheric water vapor, *Geophys. Res. Lett.*, *28*, 1551–1554, doi:10.1029/1999GL011197.

Simmons, A. S., S. Uppala, D. Dee, and S. Kobayashi (2007), ERA-Interim: New ECMWF reanalysis products from 1989 onwards, *ECMWF Newsl.*, *110*, 29–35. (Available at http://www.ecmwf.int/publications/newsletters/pdf/110_rev.pdf.)

Sinnhuber, B.-M., and I. Folkins (2006), Estimating the contribution of bromoform to stratospheric bromine and its relation to dehydration in the tropical tropopause layer, *Atmos. Chem. Phys.*, *6*, 4755–4761.

Solomon, S., K. H. Rosenlof, R. W. Portmann, J. S. Daniel, S. M. Davis, T. J. Sanford, and G.-K. Plattner (2010), Contributions of stratospheric water vapor to decadal changes in the rate of global warming, *Science*, *327*, 1219–1223.

Steinwagner, J., S. Fueglistaler, G. Stiller, T. von Clarmann, M. Kiefer, P.-P. Borsbroom, A. van Delden, and T. Röckmann (2010), Tropical dehydration processes constrained by the seasonality of stratospheric deuterated water, *Nat. Geosci.*, *3*, 262–266.

Stenke, A., and V. Grewe (2005), Simulation of stratospheric water vapor trends: Impact on stratospheric ozone chemistry, *Atmos. Chem. Phys.*, *5*, 1257–1272.

Uyeda, H., H. Yamada, J. Horikomi, R. Shirooka, S. Shimizu, L. Liu, K. Ueno, H. Fujii, and T. Koike (2001), Characteristics of convective clouds observed by a Doppler radar at Naqu on Tibetan Plateau during the GAME-Tibet IOP, *J. Meteorol. Soc. Jpn.*, *79*(1B), 463–474.

Waters, J. W., et al. (2006), The Earth Observing System Microwave Limb Sounder (EOS MLS) on the Aura satellite, *IEEE Trans. Geosci. Remote Sens.*, *44*(5), 1075–1092, doi:10.1109/TGRS.2006.873771.

Yasunari, T., and T. Miwa (2006), Convective cloud systems over the Tibetan Plateau and their impact on meso-scale disturbances in the Meiyu/Baiu frontal zone, *J. Meteorol. Soc. Jpn.*, *84*(4), 783–803.

R. Fu, Department of Geological Sciences, University of Texas at Austin, Austin, TX 78712, USA. (rongfu@jsg.utexas.edu)

S. Fueglistaler, Department of Geosciences, Princeton University, Princeton, NJ 08544, USA.

Y. S. Liu, School of Mathematics and Statistics, University of St. Andrews, North Haugh KY16 9SS, UK.

J. S. Wright, Department of Applied Mathematics and Theoretical Physics, University of Cambridge, Wilberforce Road, Cambridge CB3 0WA, UK. (j.wright@damtp.cam.ac.uk)

Y. Zhang, Goddard Earth Sciences and Technology Center, University of Maryland Baltimore County, Baltimore, MD 21228, USA.